EES Solar

PAPER

View Article Online
View Journal | View Issue

Cite this: *EES Sol.*, 2025, **1**, 1093

Mapping the surface electronic landscape of solution-processed $CuIn(S,Se)_2$ thin-films as a function of the Cu/In ratio

Ye Ma,[a] Alice Sheppard,[ab] Jacques D. Kenyon,[c] Jude Laverock,[a] Nada Benhaddou,[c] Valentina Corsetti,[a] Jake W. Bowers[c] and David J. Fermin[*a]

This study explores the influence of the Cu/In ratio, ranging from 0.80 to 1.10, on the surface composition, electronic landscape, and photovoltaic (PV) performance of solution-processed $CuIn(S,Se)_2$ (CISSe) thin films. X-ray fluorescence (XRF) confirmed that the Cu/In ratio in the CISSe films closely matches that of the precursor solution, while X-ray diffraction (XRD) indicated a consistent Se/(Se + S) ratio of 0.55 across all samples. In contrast, X-ray photoelectron spectroscopy (XPS) revealed that the surface Cu/In ratio is approximately 30% lower than the bulk value. CISSe devices fabricated in a standard substrate configuration (SLG/Mo/CISSe/CdS/i-ZnO/Al : ZnO) exhibited the highest power conversion efficiency (PCE) of 9.1% at a Cu/In ratio of 0.95. As the Cu content increased, PCE dropped sharply, accompanied by a reduction in band tailing (decrease in bulk disorder). For the first time, energy-filtered photoemission electron microscopy was used to reveal a direct correlation between PV performance and the evolution of the surface electronic landscape. The highest PCE corresponded to CISSe absorbers with a mean work function (WF) of 4.9 eV. Increasing the Cu/In ratio beyond 0.95 led to a significant decrease in mean WF. Notably, at a Cu/In ratio of 1.10, nanometer-sized domains with WF values as low as 3.9 eV emerged. These features are discussed in the context of the complex interplay between bulk and surface disorder and their impact on PV performance.

Received 11th July 2025
Accepted 6th October 2025

DOI: 10.1039/d5el00116a

rsc.li/EESSolar

Broader context

Solution-processing of inorganic thin-film absorbers offers a scalable and cost-effective route for fabricating photovoltaic devices. This method is particularly well-suited for substrates with diverse functionalities, including flexibility, transparency, and complex surface geometries. These approaches involve casting molecular precursors onto a substrate, followed by reactive annealing to form the semiconductor layer. The structure and optoelectronic properties of the compound semiconductors are sensitive to the composition, coordination chemistry, and rheological behavior of the precursor solution. $CuIn(S,Se)_2$ has garnered significant attention due to the promising power conversion efficiencies achieved in solution-processed devices. Here, we investigate how the Cu/In ratio in the precursor solution influences the structure, morphology, and photovoltaic performance of $CuIn(S,Se)_2$ devices. Our findings show that device performance markedly declines when the bulk Cu/In ratio exceeds 1.0, despite no significant changes in film structure or morphology. For the first time, we demonstrate—using energy-filtered photoemission electron microscopy—that this performance drop is linked to nanometer-sized $Cu_{2-x}Se$ surface islands exhibiting work-function values as low as 3.9 eV, which are formed even when the surface Cu/In ratio is 0.8. Our study highlights the intricate nature of the surface electronic landscape in compound semiconductors and its critical impact on photovoltaic performance.

Introduction

Chalcopyrite $Cu(In,Ga)(S,Se)_2$ (CIGSSe) and $CuIn(S,Se)_2$ (CISSe) based thin-film solar cells are some of the most promising thin-film photovoltaics (PVs) due to their high absorption coefficients, tunable and direct bandgap, and long-term stability.[1] A state-of-the-art energy conversion efficiency of 23.64% has been achieved for a CIGSSe solar cell deposited using co-evaporation.[2] In an effort towards decreasing manufacturing costs, solution-based processing methods have been considered as an alternative to vacuum deposition.[3–5] Solution-processed CISSe solar cells have surpassed 14% power conversion efficiency by conditioning the substrate surface and physical properties of the solvent in the precursor solution,[6,7] which is close to the record efficiency obtained by physical vapor deposition methods (15.0%).[8] As expected for chalcogenides, the bandgap of CISSe can be adjusted in the range of 1.04–1.53 eV by tuning the S and Se ratio,[9] and some studies

[a]School of Chemistry, University of Bristol, Cantocks Close, BS8 1TS Bristol, UK. E-mail: david.fermin@bristol.ac.uk

[b]H. H. Wills Physics Laboratory, University of Bristol, Tyndall Avenue, BS8 1TL Bristol, UK

[c]Centre for Renewable Energy Systems Technology (CREST), Wolfson School of Mechanical Electrical and Manufacturing Engineering, Loughborough University, Loughborough, LE11 3TU, UK

suggest that sulfur-containing CISSe can reduce defect densities, thus improving carrier lifetime and device stability.[10,11]

High efficiency solution-processed CISSe devices are typically linked to sub-stoichiometric Cu/In ratio of 0.90–0.95,[12,13] which have been rationalized in terms of the role of intrinsic point defects such as vacancies (V_{Cu}), interstitials (Cu_i) and antisites (In_{Cu}).[14,15] Furthermore, in Cu-poor chalcopyrite, ordered vacancy compounds (OVC, *i.e.* $CuIn_3Se_5$ or $CuIn_5Se_8$)[16,17] can be unintentionally formed during selenization. Copper selenide ($Cu_{2-x}Se$) secondary phases in Cu-rich compositions are often reported, which have a significant impact on device performance.[18] However, it has also been reported that Cu-rich CISe shows improved performance due to its passivated defects and large grain morphology.[19] Our previous analysis on solution processed CISSe, based on variable temperature admittance and photoluminescence spectroscopy, have shown significant contributions of surface recombination, identifying grain growth as a key parameter to control.[20] Consequently, there is a delicate balance of morphological and opto-electronic parameters linked to Cu/In ratio in the film which requires further investigation.

In this study, we uncover the impact of Cu/In ratio on the complex surface electronic landscape of solution processed CISSe. We first investigated the device properties, phase formation, and morphology associated with Cu/In ratios between 0.80 and 1.10. The champion device was measured with a Cu/In ratio of 0.95, exhibiting a power conversion efficiency (PCE) of 9.1% and an open-circuit voltage deficit ($V_{OC,def}$) of 431 mV. XPS analysis shows that all films are highly Cu-poor, with Cu/In ratios ranging from 0.42 to 0.62. Sub-micron resolution energy-filtered photoemission electron microscopy (EF-PEEM) shows, for the first time, complex spatial variations of the work functions which are linked to surface chemical disorder. As the bulk Cu/In ratio increases above 1, islands with work functions as low as 3.9 eV are generated across the surface, which are assigned to surface confined copper selenide phases. Our analysis concludes that the complex dependence of device performance with Cu/In ratio is the result of delicate balance between a decrease in bulk disorder and an increase in surface disorder with increasing Cu/In ratio.

Results and discussion

The impact of Cu/In ratio on PV metrics of CISSe solar devices are shown in Fig. 1a–d (see also Table S1 in the SI). As described in the experimental methods section of the SI, CISSe were prepared by sequential spin-coating steps of a precursor solution containing thiourea, CuCl, and $InCl_3$ in a 75 : 25 dimethylformamide/isopropyl alcohol mixture. As shown in our recent study on solution processed CZTSSe, this solvent mixture exhibits the appropriate rheology for deposition of homogeneous precursor films.[21] Throughout this study, CISSe absorbers will be referred to by their bulk Cu/In ratio, 0.80, 0.95, 1.00 and 1.10 obtained from X-ray fluorescence (XRF). As shown in Table S2, the XRF data follows closely the Cu/In ratio in the precursor solution. The box plots in Fig. 1a–d show that the maximum PCE is achieved in devices with Cu/In ratio of 0.95, which is primarily determined by the open circuit voltage (V_{OC}) and, to a lesser extent, fill factor (FF). Cu-rich phases also show a significant drop in the short-circuit current (J_{sc}).

Fig. 1e display illuminated and dark *J–V* curves and EQE of the champion cells for each Cu/In composition, as summarized in Table S3. CISSe solar cells with a Cu/In ratio of 0.95 gave a champion PCE of 9.1%, with V_{OC} of 533 mV, J_{sc} of 26.4 mA cm^{-2} and FF of 64.7%. The PCE decreased for absorbers with Cu/In ratios of 1.00 and 1.10, to 8.9% and 6.2%, respectively. The EQE spectra (Fig. 1f) show that current losses have contributions from the CdS absorption, reflection losses, and, as shown below, some transmission losses may also occur as the films thickness is below 600 nm. The key observation from this data is the V_{OC} deficit ($V_{OC,def}$), decreasing from 486 mV to 431 mV upon increasing the Cu/In ratio from 0.80 to 0.95, and then increasing to 504 mV for Cu/In-1.10 (Table S3), indicating that Cu/In-0.95 exhibits the lowest charge recombination losses of the series.[22] The Urbach energy (E_U) was also extracted from EQE, as displayed in Fig. 1g.[23] The E_U decreases from 21.9 to 16.9 meV with increasing Cu/In ratios, suggesting a reduction in band edge fluctuations and bulk disorder with increasing Cu content.[24] Similar observations have also been reported for co-evaporated double-graded CIGSSe absorbers.[25–27] Also, Cu-poor devices exhibit higher saturation current density, suggesting a more significant bulk recombination (Table S3). This interesting observation reveals that the overall device performance is not only determined by the bulk opto-electronic properties of the absorber.

Fig. 2a depicts the X-ray diffraction (XRD) patterns of films fabricated by different composition precursors. Regardless of the Cu/In ratio, the (112), (220) and (312) crystallographic planes located at around 27.1°, 46.5°, and 53.5° support the presence of polycrystalline CISSe phase (JCPDS 65-2732 and JCPDS 87-2265). Fig. S1 examines more closely the range of 20° to 40°, confirming that no diffraction features attributed to Cu_2Se and In_2Se_3 secondary phases are observed in this range. Based on the peak position, the estimated Se/(Se + S) of all CISSe absorber is around 0.55, indicating a high replacement of sulfur by selenium and consistent with the band gap values estimated from EQE. Fig. 2b shows the Raman spectra, where the films exhibited characteristic CISe (175 and 220 cm^{-1}) and CIS (295 and 320 cm^{-1}) peaks. The peak at 159 cm^{-1} is within resonant range of $CuIn_3Se_5$ OVC.[17,28] Fig. S2 shows the normalized peak ratio of the OVC-related mode to CISSe A^1 mode decreasing with increasing Cu/In ratio, indicating OVCs are more prevalent with Cu-poor films.[29,30] It should be mentioned that Cu_2Se phases are characterized by broad features Raman bands at 260 and 290 cm^{-1}, while CuSe exhibits well defined strong Raman features at 260, 320 and 470 cm^{-1}.[31–37] None of these Raman modes are observed in the spectra shown in Fig. 2b, regardless of the Cu/In ratio.

The top-down SEM images of the CISSe thin-films with various Cu/In ratios are shown in Fig. 3a–d, exhibiting densely packed polygonal grains for all samples. Although few smaller grains are observed in Cu/In 0.80 films, no systematic changes in the thin-films morphology can be seen with an increasing Cu/In ratio. Cross-sectional SEM images (Fig. 3e–h) exhibit high

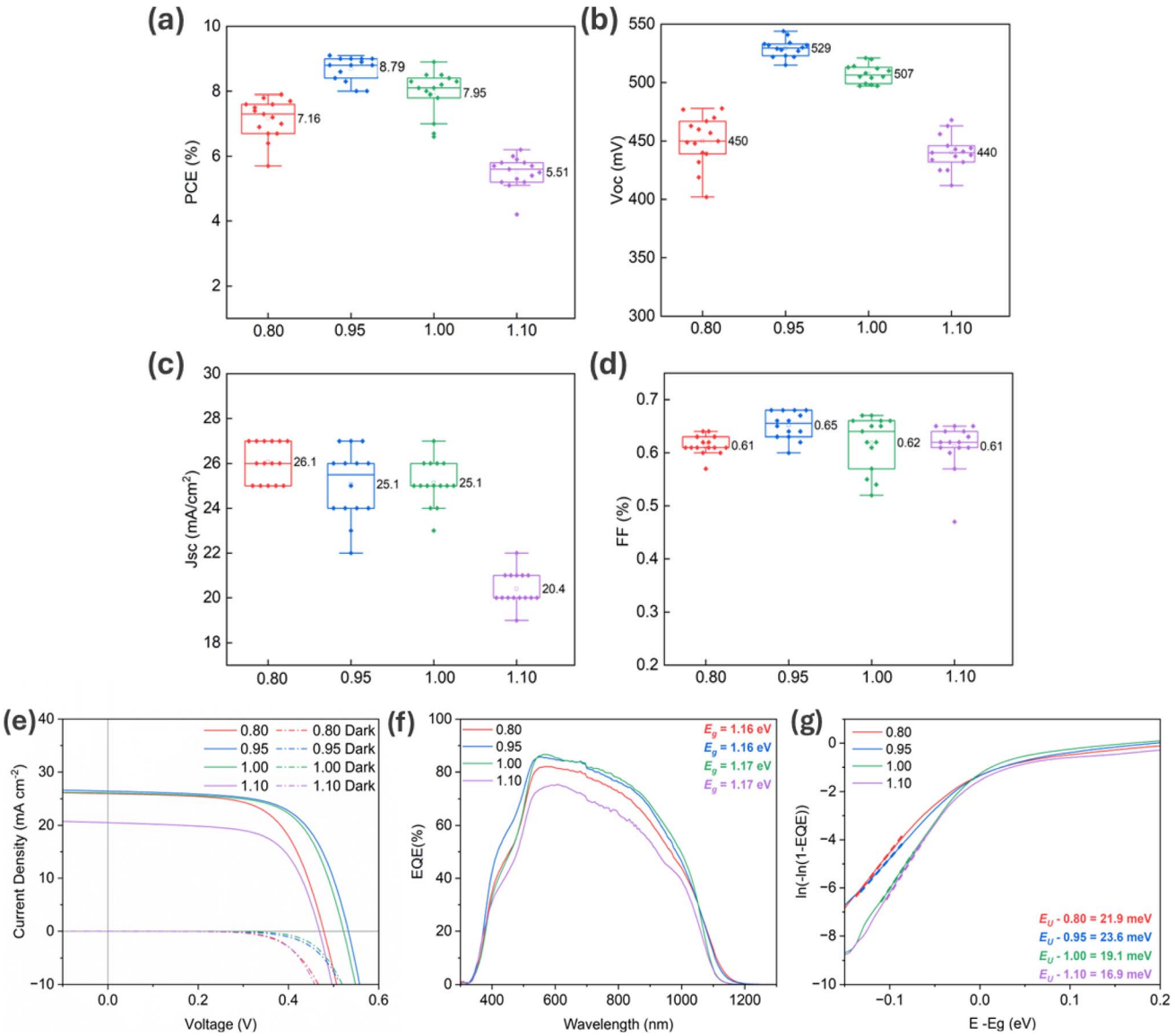

Fig. 1 (a–d) Statistical distribution of the photovoltaic parameters for devices with varying Cu/In ratios. (e) Illuminated and dark *J*–*V* and (f) external quantum efficiency (EQE) characteristics of champion devices with varying Cu/In ratios, along with (g) plots of ln(−ln(1 − EQE)) *versus* *E*–E_g extracted from EQE.

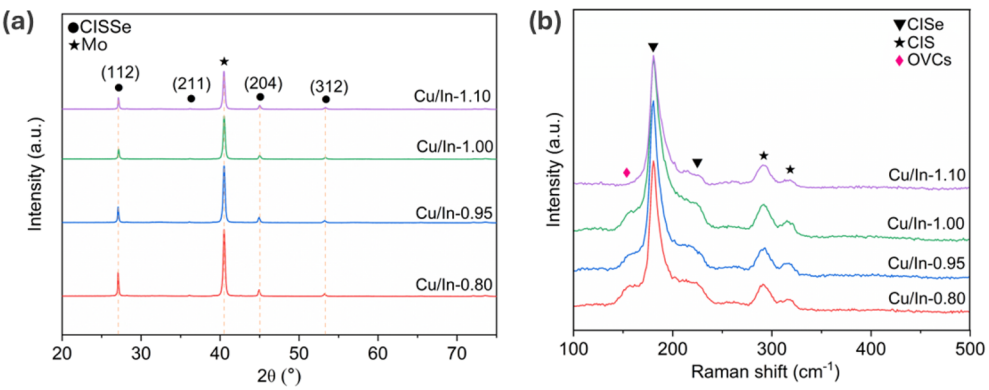

Fig. 2 (a) XRD patterns and (b) Raman spectra with 488 nm excitation laser of Cu/In-0.80 (red), Cu/In-0.95 (blue), Cu/In-1.00 (green), Cu/In-1.10 films (purple).

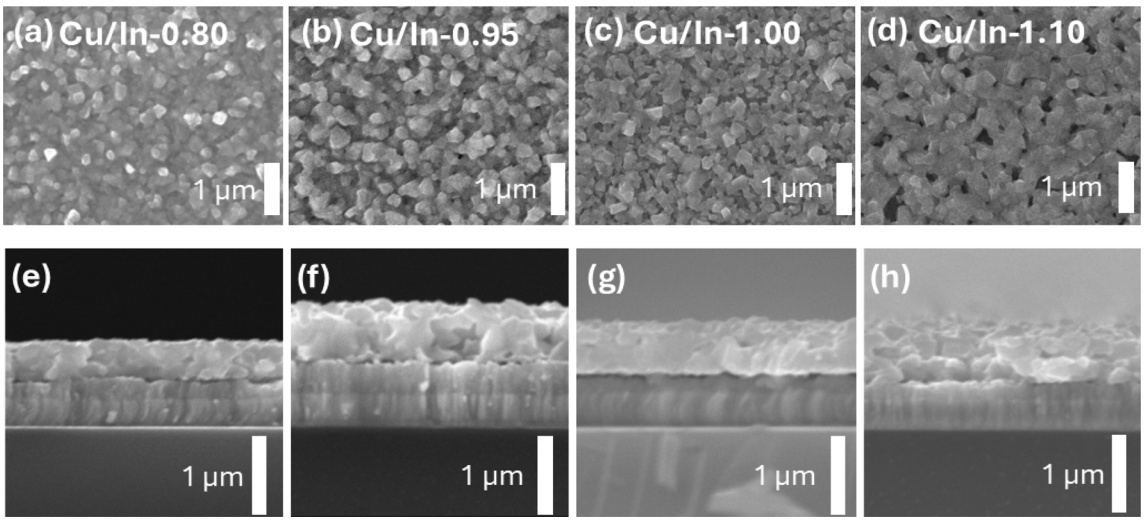

Fig. 3 Top-view SEM images of Cu/In-0.80 (a), Cu/In-0.95 (b), Cu/In-1.00 (c), Cu/In-1.10 absorbers (d). Cross-section SEM images of Cu/In-0.80 (e) Cu/In-0.95 (f), Cu/In-1.00 (g), Cu/In-1.10 absorbers (h).

compact films with a thickness ranging from 550 to 580 nm. An additional contrast in the cross-section analysis can be seen in the boundary between the absorber and the Mo support, which is associated with the $Mo(S,Se)_x$ formed during selenization step. It is important to mention that the addition of SeS_2 to the graphite box regulates the excessive selenization of the Mo layer observed in our previous work, at the expense of S content in the film, which increases the band gap.[20]

Fig. 4a and b shows the X-ray photoelectron spectroscopy (XPS) of Cu 2p and In 3d as a function of the bulk Cu/In ratio. The Cu and In peak position, broadening and orbital splitting are similar for all compositions, corresponding to Cu^+ and In^{3+}, respectively.[38] Fig. S3a and b show the Se 3d and S 2p/Se 3p XPS spectra, which are comparable for all samples. Interestingly, a low intensity Na 1s peak is observed arising from the diffusion of Na from the SLG during rapid thermal annealing (Fig. S3c).[39] As described in Experimental methods (SI), the films were pre-treated using Ar^+ to remove surface contaminants. Fig. S4 shows the XPS spectra of Se 3d for sample Cu/In-0.80 before and after surface pretreatment, confirming that adventitious oxygen residuals and contaminates are successfully removed. Fig. 4a and b also shows a correlation between the intensity of Cu 2p, In 3d and the bulk Cu/In precursor ratio.[39] As displayed in Fig. 4c, the surface Cu/In ratio extracted from the XPS spectra show a significant Cu depletion, with values approximately 30% lower than in the bulk. As shown in Fig. S5, Cu 2p and In 3d spectrum of the Cu/In-1.00 absorber are used to demonstrate the data analysis procedure. Cu surface depletion has been extensively reported in the presence of alkali elements, which can generate surface confined alkali-In–Se.[25,40–47] Alkali-In–Se secondary phases have been linked to a decrease in interfacial recombination rate, thus increasing V_{OC} and FF.[48] Fig. S6 illustrates the elemental distribution across the Cu/In-0.95. The data confirms the presence of Na across the film, as well as relatively homogeneous distributions of Cu and In in a ratio consistent with the XRF analysis (Table S2). These observations confirm the diffusion of Na from the substrate upon annealing.

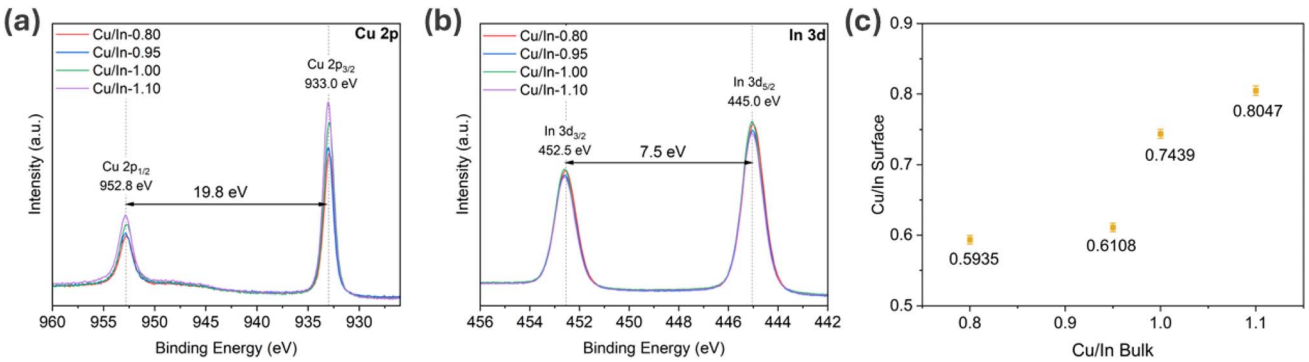

Fig. 4 XPS binding energy profiles of (a) Cu 2p and (b) In 3d for CISSe absorbers of Cu/In-0.80 (red), Cu/In-0.95 (blue), Cu/In-1.00 (green), and Cu/In-1.10 (purple) ratios. (c) Cu/In surface ratio as a function of Cu/In bulk ratio. Error bars in (c) represent statistical errors associated with determining the peak areas.

Fig. 5 shows sub-micron resolution effective work function (WF) maps constructed from energy-filtered photoemission electron microscopy (EF-PEEM) analysis of CISSe absorbers with the various Cu/In ratio. EF-PEEM maps were recorded under monochromatic He I excitation (21.22 eV) with a spatial resolution of 100 nm. The 20 μm × 20 μm field map provides a wealth of information in relation to the surface electronic landscape of CISSe. As shown in Fig. S7 and Table S4, fitting the WF spatial distribution to a Gaussian function enables us to quantify the center of the distribution and the standard deviation which can be linked to spatial inhomogeneities in the surface electronic landscape. Cu/In-0.80 shows a narrow spatial distribution of WF centered at 4.85 eV, which increases to 4.90 eV for Cu/In-0.95. As the Cu content further increases, the center of the WF distribution sharply drops to 4.55 eV. It is interesting to notice that the non-monotonic trend of WF center with Cu/In ratio mirrors the trend of the device V_{OC}, as discussed further below. The standard deviation also exhibits a complex dependence with the Cu–In ratio, varying between 54 to 102 meV. However, the most striking aspect in this analysis is the long tail towards low WF values observed in the case of Cu/In-1.10. The number of WF counts below 4.3 eV is several orders of magnitude smaller than the WF center, indicating that these are localized nanometer scale domains. The emergence of these domains coincides with the drastic drop in device performance. A variety of parameters can affect the spatial distribution of WF, including topography, local surface potentials and surface confined phases contributions.[21,49–52] However, given that the topographic features of the films are rather similar across the composition range, the low WF hot-spots can be linked to surface confined $Cu_{2-x}Se$ phases which are characterized by WF values in the range of 3 eV.[53–55] Although it could be expected that the formation of these secondary phases would take place at higher Cu content, it is important to consider that the film surfaces are substantially Cu depleted in comparison to the bulk. As concluded from the Raman analysis (Fig. 2b), there is no evidence of binary Cu chalcogenide phases observed in the bulk. These features are extraordinarily difficult to probe by other techniques just by the virtue of being confined to discreet sub-micron islands at the surface of the absorber.

Fig. 6a contrasts the ultraviolet photoelectron spectra (UPS) of the CISSe films as a function of the Cu/In ratio. Cu/In-0.80 and Cu/In-0.95 exhibits broad features in the valence band (VB) spectra centered at 4.5 and 7.5 eV, which are in good agreement with spectra reported of Cu-poor CISSe.[56–58] These features clearly sharpen in Cu/In-1.00 films, which is consistent with VB spectra reported in $CuInSe_2$.[59] The lineshape of the VB spectrum changes significantly for Cu/In-1.10, extending beyond 10 eV in the binding energy scale. These features clearly sharpen in Cu/In-1.00 films, which is consistent with VB spectra

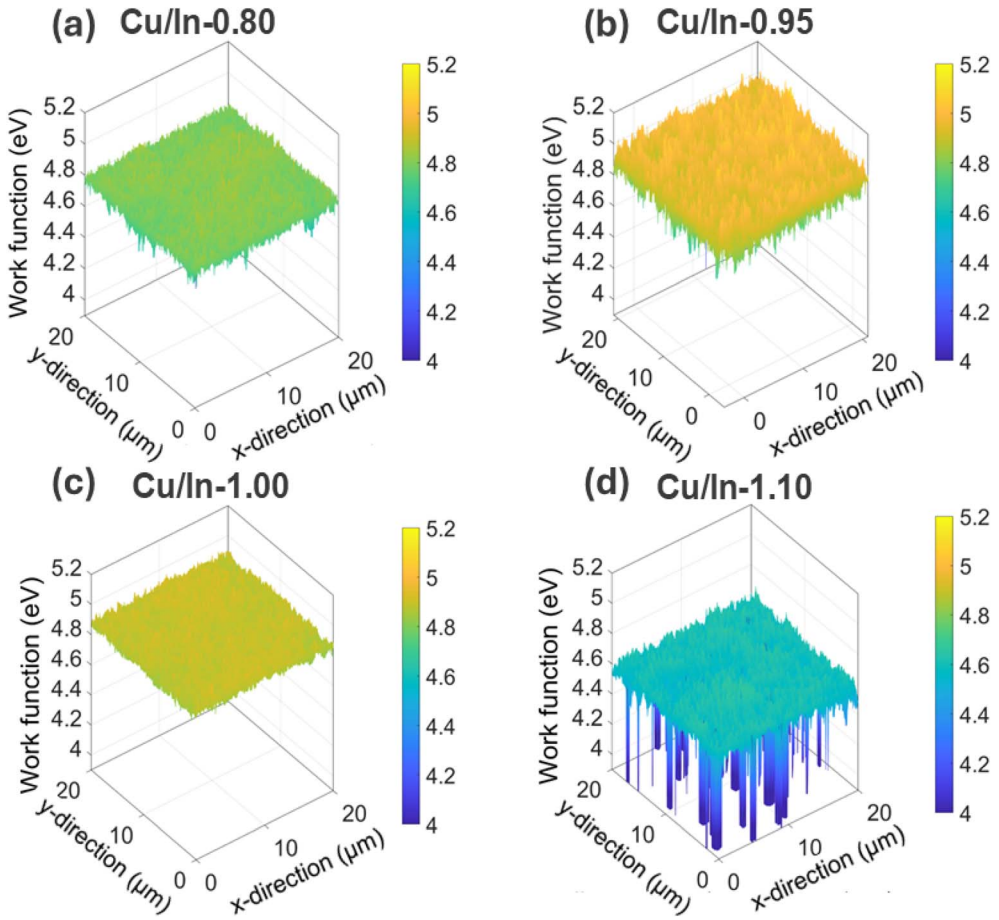

Fig. 5 3D photoemission WF maps of the Cu/In-0.80 (a), Cu/In-0.95 (b), Cu/In-1.00 (c), Cu/In-1.10 (d) CISSe films.

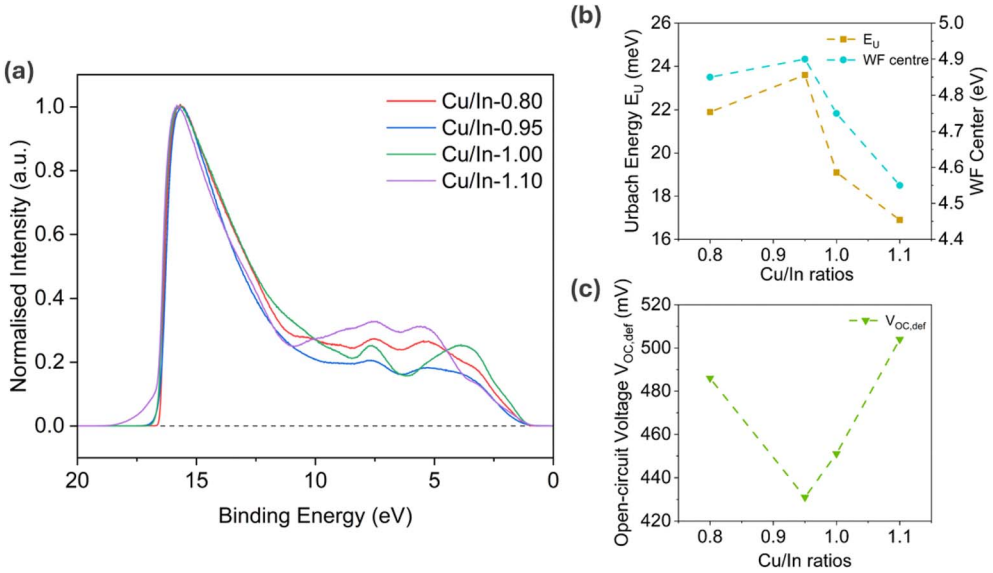

Fig. 6 (a) Normalized UPS spectra of the CISSe absorbers of Cu/In-0.80 (red), Cu/In-0.95 (blue), Cu/In-1.00 (green), Cu/In-1.10 ratios (purple). (b) Summarized Urbach Energy, WF center and (c) $V_{OC,def}$ as a function of Cu/In ratios.

reported in $CuInSe_2$.[59] The lineshape of the VB spectrum changes significantly for Cu/In-1.10, extending beyond 10 eV in the binding energy scale. This spectral responses exhibit similar features to those reported for Cu_2Se.[60,61] Furthermore, a tail in the onset of electron photoemission is observed in the Cu/In-1.10 spectrum, consistent with tail in WF values. These observations provide further evidence that the regions of low WF observed in the EF-PEEM maps are associated with surface confined sub-micrometer Cu_xSe phases.

As displayed in Fig. 6b and c, the combination of EF-PEEM data and PV device metrics reveal some important aspects in relation to the composition dependence of CISSe thin films. As Cu/In increases, we observed a close correlation between E_U and WF center, revealing a complex relation between bulk disorder, ordered vacancy compounds (OVC) and the Fermi level. Cu-poor chalcopyrite contains OVCs as well as In_{Cu} antisites,[19,62] while increasing the Cu content leads to more ordered structures with larger grains.[18] On the other hand, Fig. 6c shows that the $V_{OC,def}$ sharply increases as the bulk Cu/In ratio increases above 0.95, which is also consistent with previous studies on high efficiency CISSe.[63] EF-PEEM reveals a broadening of the spatial distribution of WF values, with evidence of the formation of surface confined binary Cu chalcogenides phases as the surface Cu/In ratio increases just above 80%.[63] EF-PEEM reveals a broadening of the spatial distribution of WF values, with evidence of the formation of surface confined binary Cu chalcogenides phases as the surface Cu/In ratio increases just above 80%. This behavior could be the manifestation of the transport rates of Cu^+ *vs.* Na^+ under our specific annealing conditions. Consequently, we anticipate that introducing alkali ions in the precursor solution, sodium content in the substrate and annealing temperature can significantly affect the emergence of these low WF surface sites.

Conclusions

This work reveals a complex relationship between bulk and surface disorder in solution-processed CISSe thin films and its impact on optoelectronic properties and photovoltaic performance. The highest PCE was achieved at a Cu/In ratio of 0.95, which also exhibited the highest V_{OC} in the series. As the Cu/In ratio increased, both V_{OC} and J_{sc} declined significantly, despite no observable changes in bulk structural parameters. Interestingly, band tailing, estimated from EQE spectra, systematically decreased with increasing Cu/In ratio.

Bulk composition analysis confirmed a strong 1 : 1 correlation between the Cu/In ratio in the precursor solution and the annealed CISSe films. However, XPS revealed a substantial depletion of Cu at the surface, with surface Cu/In ratios approximately 30% lower than in the bulk. EF-PEEM analysis showed that the mean surface WF peaked at 4.90 eV for a Cu/In ratio of 0.95, then dropped to 4.55 eV at higher Cu content. Most notably, nanoscale-sized domains with WF values as low as 3.9 eV appeared at a Cu/In ratio of 1.10. These domains are attributed to surface-confined $Cu_{2-x}Se$ islands, which form even when the surface remains Cu-poor. Although these highly confined islands are undetectable by conventional techniques, such as Raman spectroscopy, they exert considerable influence on PV device performance.

Author contributions

Y. Ma wrote the manuscript, fabricated and characterized the CISSe absorbers, data curation and analysis. A. Sheppard and V. Corsetti provided scientific discussions and aided data interpretation, reviewed and edited the manuscript. J. Kenyon, N. Benhaddou and J. W. Bowers contributed to CISSe device fabrication, and JV and EQE measurements. J. Laverock aided in the acquisition and analysis of XPS and EF-PEEM

measurements. D. J. Fermin contributed to the manuscript preparation, data analysis and supervised the research project. All authors were involved in the discussions and approved of the manuscript.

Conflicts of interest

The authors declare that there are no conflicts of interest.

Data availability

Data are available at the University of Bristol data repository, data.bris, at **https://doi.org/10.5523/bris.3mho5r38ai5k02ro43vzhat07y**.

Supplementary information: Experimental methods; Table S1 – average device metrics as a function of the bulk Cu/In ratio; Table S2 – Cu/In ratio in the precursor solution *vs.* thin-film measured by XRF; Table S3 – best device metrics as a function of the bulk Cu/In ratio; Table S4 – surface Cu/In ratio estimated from XPS and WF center obtained from EF-PEEM; Fig. S1 – XRD patterns in the range of 20 to 40°; Fig. S2 – normalized peak area of OVCs mode to CISe A^1 mode of each Cu/In ratio; Fig. S3 – XPS spectra of (a) Se 3d, (b) S 2p and Se 3p, and (c) Na 1s of the CISSe absorbers; Fig. S4 – XPS spectra of Se 3d for Cu/In-0.80 absorber before and after surface pretreatment; Fig. S5 – extended (raw) spectrum, background based on energy loss theory, and background-subtracted spectrum used for quantification of Cu 2p and In 3d of absorber Cu/In-1.00; Fig. 6 – secondary ion mass spectrometry (SIMS) profile of Cu/In-0.95 absorber; Fig. S7 – the WF histograms of the CISSe absorber as a function of the bulk Cu/In ratio; Raw data are also available at the University of Bristol data repository, data.bris, at **https://doi.org/10.5523/bris.3mho5r38ai5k02ro43vzhat07y**. See DOI: **https://doi.org/10.1039/d5el00116a**.

Acknowledgements

Y. Ma is grateful for China Scholarship Council (File No. 202208610015). A. Sheppard acknowledges the financial support of the Engineering and Physical Sciences Research Council (EPSRC, DTA grant EP/T517872/1). V. Corsetti is grateful to the University of Bristol for the Strategic PhD Scholarship 2023. D. J. Fermin acknowledges the support from EPSRC through the SolPV grant EP/V008676/1. N. Benhaddou and J. W. Bowers are grateful through the support *via* EP/V008692/1. The authors acknowledge use of the University of Bristol NanoESCA II Laboratory.

References

1 J. Ramanujam and U. P. Singh, Copper indium gallium selenide based solar cells - A review, *Energy Environ. Sci.*, 2017, **10**, 1306–1319.
2 J. Keller, K. Kiselman, O. Donzel-Gargand, N. M. Martin, M. Babucci, O. Lundberg, E. Wallin, L. Stolt and M. Edoff, High-concentration silver alloying and steep back-contact gallium grading enabling copper indium gallium selenide solar cell with 23.6% efficiency, *Nat. Energy*, 2024, **9**, 467–478.
3 R. N. Bhattacharya, J. F. Hiltner, W. Batchelor, M. A. Contreras, R. N. Noufi and J. R. Sites, 15.4% CuIn1−xGaxSe2-based photovoltaic cells from solution-based precursor films, *Thin Solid Films*, 2000, **361–362**, 396–399.
4 T. Zhang, Y. Yang, D. Liu, S. C. Tse, W. Cao, Z. Feng, S. Chen and L. Qian, High efficiency solution-processed thin-film Cu(In,Ga)(Se,S)2 solar cells, *Energy Environ. Sci.*, 2016, **9**, 3674–3681.
5 T. Feurer, R. Carron, G. Torres Sevilla, F. Fu, S. Pisoni, Y. E. Romanyuk, S. Buecheler and A. N. Tiwari, Efficiency Improvement of Near-Stoichiometric CuInSe2 Solar Cells for Application in Tandem Devices, *Adv. Energy Mater.*, 2019, **9**, 1901428.
6 S. Suresh, A. T. Gidey, T. H. Chowdhury, S. R. Rondiya, L. Tao, J. Liu, B. Vermang and A. R. Uhl, Rear Surface Passivation for Ink-Based, Submicron CuIn(S, Se)2 Solar Cells. Adv, *Energy Mater.*, 2024, **14**, 2303309.
7 Y. Siddique, K. Son, T. R. Rana, S. D. H. Naqvi, P. M. Hoang, A. Ullah, H. Tran, S. M. Lee, S. Hong, S. K. Ahn, I. Jeong and S. Ahn, Air-processable high-efficiency CISSe solar cells from DMF molecular solution and their application to perovskite/CISSe tandems, *Energy Environ. Sci.*, 2022, **15**, 1479–1492.
8 A. Jehad, R. Noufi, S. Johnston, S. Ward and X. Wu, Jan, Improved performance in CuInSe2 and Surface-modified CuGaSe2 solar cells, *Conf. Rec. IEEE Photovoltaic Spec. Conf.*, 2005, **02**, 299–302.
9 R. Félix, A. Weber, O. Zander, H. Rodriguez-Álvarez, B.-A. Schubert, J. Klaer, R. G. Wilks, H.-W. Schock, R. Mainz and M. Bär, Selenization of CuInS2 by rapid thermal processing – an alternative approach to induce a band gap grading in chalcopyrite thin-film solar cell absorbers?, *J. Mater. Chem. A*, 2019, **7**, 2087–2094.
10 T. Lavrenko, T. Ott and T. Walter, Impact of sulfur and gallium gradients on the performance of thin film Cu(In,Ga)(Se,S)2 solar cells, *Thin Solid Films*, 2015, **582**, 51–55.
11 S. Yuan, X. Wang, Y. Zhao, Q. Chang, Z. Xu, J. Kong and S. Wu, Solution Processed Cu(In,Ga)(S,Se)2 Solar Cells with 15.25% Efficiency by Surface Sulfurization, *ACS Appl. Energy Mater.*, 2020, **3**, 6785–6792.
12 S. Suresh and A. R. Uhl, Present Status of Solution-Processing Routes for Cu(In,Ga)(S,Se)2 Solar Cell Absorbers, *Adv. Energy Mater.*, 2021, **14**, 2003743.
13 L. Choubrac, E. Bertin, F. Pineau, L. Arzel, T. Lepetit, L. Assmann, T. Aloui, S. Harel and N. Barreau, On the role of sodium and copper off-stoichiometry in Cu (In,Ga)S2 for photovoltaic applications: Insights from the investigation of more than 500 samples, *Prog. Photovolt. Res. Appl.*, 2023, **31**, 971–980.
14 S. Schuler, S. Siebentritt, S. Nishiwaki, N. Rega, J. Beckmann, S. Brehme and M. C. Lux-Steiner, Self-compensation of intrinsic defects in the ternary semiconductor CuGaSe2, *Phys. Rev. B:Condens. Matter Mater. Phys.*, 2004, **69**, 045210.

15 J. Krustok, H. Collan, M. Yakushev and K. Hjelt, The role of spatial potential fluctuations in the shape of the PL bands of multinary semiconductor compounds, *Phys. Scr.*, 1999, **1999**, 179.
16 T. Maeda, W. Gong and T. Wada, CuInSe2, CuIn3Se5, and CuIn5Se8 phases in Cu-poor Cu2Se–In2Se3 pseudo-binary system – Their crystal structures, optical properties and electronic structures, *Curr. Opin. Green Sustainable Chem.*, 2017, **4**, 77–83.
17 S. B. Zhang, S.-H. Wei and A. Zunger, Stabilization of Ternary Compounds via Ordered Arrays of Defect Pairs, *Phys. Rev. Lett.*, 1997, **78**, 4059–4062.
18 S. Shukla, M. Sood, D. Adeleye, S. Peedle, G. Kusch, D. Dahliah, M. Melchiorre, G.-M. Rignanese, G. Hautier, R. Oliver and S. Siebentritt, Over 15% efficient wide-band-gap Cu(In,Ga)S2 solar cell: Suppressing bulk and interface recombination through composition engineering, *Joule*, 2021, **5**, 1816–1831.
19 D. Abou-Ras, Microscopic origins of radiative performance losses in thin-film solar cells at the example of (Ag,Cu)(In,Ga)Se2 devices, *J. Vac. Sci. Technol., A*, 2024, **42**, 022803.
20 D. Tiwari, T. Koehler, X. Lin, A. Sarua, R. Harniman, L. Wang, R. Klenk and D. J. Fermin, Single Molecular Precursor Solution for CuIn(S,Se)2 Thin Films Photovoltaic Cells: Structure and Device Characteristics, *ACS Appl. Mater. Interfaces*, 2017, **9**, 2301–2308.
21 A. Sheppard, R. Agbenyeke, J. Laverock, L. King, J. Kenyon, N. Benhaddou, N. Fleck, R. L. Harniman, A. Sarua, D. Tiwari, J. W. Bowers, N. A. Fox and D. J. Fermin, Utilizing Solvent Repulsion between Dimethylformamide and Isopropanol to Manipulate Sn Distribution for Bifacial Cu2ZnSn(S,Se)4 Solar Cells, *ACS Appl. Energy Mater.*, 2024, **7**, 11766–11774.
22 R. Gutzler, W. Witte, A. Kanevce, D. Hariskos and S. Paetel, VOC-losses across the band gap: Insights from a high-throughput inline process for CIGS solar cells, *Prog. Photovolt. Res. Appl.*, 2023, **31**, 1023–1031.
23 S. Hadke, S. Levcenko, G. Sai Gautam, C. J. Hages, J. A. Márquez, V. Izquierdo-Roca, E. A. Carter, T. Unold and L. H. Wong, Suppressed Deep Traps and Bandgap Fluctuations in Cu2CdSnS4 Solar Cells with ≈8% Efficiency, *Adv. Energy Mater.*, 2019, **9**, 1902509.
24 A. Guchhait, Z. Su, Y. F. Tay, S. Shukla, W. Li, S. W. Leow, J. M. R. Tan, S. Lie, O. Gunawan and L. H. Wong, Enhancement of Open-Circuit Voltage of Solution-Processed Cu2ZnSnS4 Solar Cells with 7.2% Efficiency by Incorporation of Silver, *ACS Energy Lett.*, 2016, **1**, 1256–1261.
25 A. Chirilă, P. Reinhard, F. Pianezzi, P. Bloesch, A. R. Uhl, C. Fella, L. Kranz, D. Keller, C. Gretener, H. Hagendorfer, D. Jaeger, R. Erni, S. Nishiwaki, S. Buecheler and A. N. Tiwari, Potassium-induced surface modification of Cu(In,Ga)Se2 thin films for high-efficiency solar cells, *Nat. Mater.*, 2013, **12**, 1107–1111.
26 R. Carron, S. Nishiwaki, T. Feurer, R. Hertwig, E. Avancini, J. Löckinger, S.-C. Yang, S. Buecheler and A. N. Tiwari, Advanced Alkali Treatments for High-Efficiency Cu(In,Ga)Se2 Solar Cells on Flexible Substrates, *Adv. Energy Mater.*, 2019, **9**, 1900408.
27 S. Siebentritt, L. Gütay, D. Regesch, Y. Aida and V. Deprédurand, Why do we make Cu(In,Ga)Se2 solar cells non-stoichiometric?, *Sol. Energy Mater. Sol. Cells*, 2013, **119**, 18–25.
28 A. J. C. M. Prot, M. Melchiorre, F. Dingwell, A. Zelenina, H. Elanzeery, A. Lomuscio, T. Dalibor, M. Guc, R. Fonoll-Rubio, V. Izquierdo-Roca, G. Kusch, R. A. Oliver and S. Siebentritt, Composition variations in Cu(In,Ga)(S,Se)2 solar cells: Not a gradient, but an interlaced network of two phases, *APL Mater.*, 2023, **11**, 101120.
29 S. Schuler, S. Siebentritt, S. Nishiwaki, N. Rega, J. Beckmann, S. Brehme and M. C. Lux-Steiner, Self-compensation of intrinsic defects in the ternary semiconductor CuGaSe2, *Phys. Rev. B:Condens. Matter Mater. Phys.*, 2004, **69**, 045210.
30 J. Krustok, H. Collan, M. Yakushev and K. Hjelt, The Role of Spatial Potential Fluctuations in the Shape of the PL Bands of Multinary Semiconductor Compounds, *Phys. Scr.*, 1999, **79**, 179.
31 R. D. Heyding and R. M. Murray, The crystal structures of $Cu_{1.8}Se$, Cu3Se2, α- and γCuSe, CuSe2, and CuSe2II, *Can. J. Chem.*, 1976, **54**, 841–848.
32 K. Yamamoto and S. Kashida, X-ray study of the average structures of Cu2Se and Cu1.8S in the room temperature and the high temperature phases, *J. Solid State Chem.*, 1991, **93**, 202–211.
33 A. V. Dooglav, R. R. Gainov, I. N. Penkov, A. Y. Orlova, I. A. Evlampiev, N. N. Mozgova and R. R. Khasanov, in *Superconductor*, ed. A. M. Luiz, IntechOpen, Rijeka, 2010.
34 Y. Jiang, Y. Xu, Q. Zhang, X. Zhao, F. Xiao, X. Wang and G. Ma, Templated Synthesis of Cu2S Hollow Structures for Highly Active Ozone Decomposition, *Catalysts*, 2024, **14**, 153.
35 Y. Zhang, X. Shao, Y. Zheng, L. Yan, P. Zhu, Y. Li and H. Xu, Pressure-induced structural transitions and electronic topological transition of Cu2Se, *J. Alloys Compd.*, 2018, **732**, 280–285.
36 I. G. Shitu, J. Y. C. Liew, Z. A. Talib, H. Baqiah, M. M. Awang Kechik, M. Ahmad Kamarudin, N. H. Osman, Y. J. Low and I. I. Lakin, Influence of Irradiation Time on the Structural and Optical Characteristics of CuSe Nanoparticles Synthesized via Microwave-Assisted Technique, *ACS Omega*, 2021, **6**, 10698–10708.
37 G. Kim, D. W. Jeong, G. Lee, S. Lee, K. Y. Ma, H. Hwang, S. Jang, J. Hong, S. Pak, S. Cha, D. Cho, S. Kim, J. Lim, Y.-W. Lee, H. S. Shin, A.-R. Jang and J.-O. Lee, Unusual Raman Enhancement Effect of Ultrathin Copper Sulfide, *Small*, 2024, **20**, 2306819.
38 N. Maticiuc, T. Kodalle, J. Lauche, R. Wenisch, T. Bertram, C. A. Kaufmann and I. Lauermann, In vacuo XPS investigation of Cu(In,Ga)Se2 surface after RbF post-deposition treatment, *Thin Solid Films*, 2018, **665**, 143–147.
39 Y. J. Jang, J. Lee, K.-B. Lee, D. Kim and Y. Lee, Quantitative Analysis and Band Gap Determination for CIGS Absorber Layers Using Surface Techniques, *J. Anal. Methods Chem.*, 2018, **2018**, 6751964.

40 D. Colombara, H. Elanzeery, N. Nicoara, D. Sharma, M. Claro, T. Schwarz, A. Koprek, M. H. Wolter, M. Melchiorre, M. Sood, N. Valle, O. Bondarchuk, F. Babbe, C. Spindler, O. Cojocaru-Miredin, D. Raabe, P. J. Dale, S. Sadewasser and S. Siebentritt, Chemical instability at chalcogenide surfaces impacts chalcopyrite devices well beyond the surface, *Nat. Commun.*, 2020, **11**, 3634.

41 Y.-H. Chen, R.-T. Kuo, W.-C. Lin, C.-Y. Lai and T.-Y. Lin, Cesium Modulation in Cu(In, Ga)(S, Se)2 Solar Cells: Comprehensive Analysis on Interface, Surface, and Grain Boundary, *ACS Appl. Mater. Interfaces*, 2024, **16**, 32220–32231.

42 C. K. Boumenou, H. Phirke, J. Rommelfangen, J.-N. Audinot, S. Nishiwaki, T. Wirtz, R. Carron and A. Redinger, Nanoscale Surface Analysis Reveals Origins of Enhanced Interface Passivation in RbF Post Deposition Treated CIGSe Solar Cells, *Adv. Funct. Mater.*, 2023, **33**, 2300590.

43 H. A. Al-Thani, M. M. Abdullah and F. S. Hasoon, Interface Investigation of ZnO/CdS/CuIn1−xGaxSe2/Mo Solar Cells, *MRS Online Proc. Libr.*, 2011, **668**, 68.

44 A. Loubat, S. Béchu, M. Bouttemy, J. Vigneron, D. Lincot, J.-F. Guillemoles and A. Etcheberry, Cu depletion on Cu(In,Ga)Se2 surfaces investigated by chemical engineering: An x-ray photoelectron spectroscopy approach, *J. Vac. Sci. Technol., A*, 2019, **37**, 041201.

45 P. Jackson, R. Wuerz, D. Hariskos, E. Lotter, W. Witte and M. Powalla, Effects of heavy alkali elements in Cu(In,Ga) Se2 solar cells with efficiencies up to 22.6%, *Phys. Status Solidi RRL*, 2016, **10**, 583–586.

46 J. Keller, H. Aboulfadl, L. Stolt, O. Donzel-Gargand and M. Edoff, Rubidium Fluoride Absorber Treatment for Wide-Gap (Ag,Cu)(In,Ga)Se2 Solar Cells, *Sol. RRL*, 2022, **6**, 2200044.

47 A. Stokes, M. Al-Jassim, D. Diercks, A. Clarke and B. Gorman, Impact of Wide-Ranging Nanoscale Chemistry on Band Structure at Cu(In, Ga)Se2 Grain Boundaries, *Sci. Rep.*, 2017, **7**, 14163.

48 N. M. Martin, T. Törndahl, E. Wallin, K. A. Simonov, H. Rensmo and C. Platzer-Björkman, Surface/Interface Effects by Alkali Postdeposition Treatments of (Ag,Cu)(In,Ga)Se2 Thin Film Solar Cells, *ACS Appl. Energy Mater.*, 2022, **5**, 461–468.

49 D. Tiwari, M. Cattelan, R. L. Harniman, A. Sarua, A. Abbas, J. W. Bowers, N. A. Fox and D. J. Fermin, Mapping Shunting Paths at the Surface of Cu2ZnSn(S,Se)4 Films via Energy-Filtered Photoemission Microscopy, *iScience*, 2018, **9**, 36–46.

50 D. Tiwari, M. Cattelan, R. L. Harniman, A. Sarua, N. Fox, T. Koehler, R. Klenk and D. J. Fermin, Impact of Sb and Na Doping on the Surface Electronic Landscape of Cu2ZnSnS4 Thin Films, *ACS Energy Lett.*, 2018, **3**, 2977–2982.

51 D. Tiwari, M. V. Yakushev, T. Koehler, M. Cattelan, N. Fox, R. W. Martin, R. Klenk and D. J. Férmin, Mapping the Energetics of Defect States in Cu2ZnSnS4 films and the Impact of Sb Doping, *ACS Appl. Energy Mater.*, 2022, **5**, 3933–3940.

52 J. S. Adu, A. Sheppard, R. E. Agbenyeke, G. K. Asare, B. H. Hamadani, D. J. Fermin and H. H. Park, Tuning the Surface Electronic Landscape of Ultrathin (Al,Sn)Ox Electron Extraction Layers in Perovskite Solar Cells, *Small*, 2025, **21**, 2412702.

53 N. M. Khusayfan and H. K. Khanfar, Structural and optical properties of Cu2Se/Yb/Cu2Se thin films, *Results Phys.*, 2019, **12**, 645–651.

54 P. Lukashev, W. R. L. Lambrecht, T. Kotani and M. van Schilfgaarde, Electronic and crystal structure of Cu2-xS: Full-potential electronic structure calculations, *Phys. Rev. B:Condens. Matter Mater. Phys.*, 2007, **76**, 195202.

55 O. Schalm, A. Patelli, P. Storme, A. Crabbé, S. Voltolina, V. Feyer and H. Terryn, A dataset of high-resolution synchrotron x-ray photoelectron spectra of tarnished silver-copper surfaces before and after reduction with a remote helium plasma at atmospheric pressure, *Data Brief*, 2021, **35**, 106872.

56 T. Schulmeyer, R. Hunger, R. Fritsche, B. Jäckel, W. Jaegermann, A. Klein, R. Kniese and M. Powalla, Interfaces of chalcogenide solar cells: a study of the composition at the Cu(In,Ga)Se2/CdS contact, *Thin Solid Films*, 2005, **480–481**, 110–117.

57 C. Rincón and R. Márquez, Defect physics of the CuInSe2 chalcopyrite semiconductor, *J. Phys. Chem. Solids*, 1999, **60**, 1865–1873.

58 S.-H. Han, C. Persson, F. S. Hasoon, H. A. Al-Thani, A. M. Hermann and D. H. Levi, Optical properties and electronic structures of ((4CuInSe2)yCuIn5Se8)1-y, *Phys. Rev. B:Condens. Matter Mater. Phys.*, 2006, **74**, 085212.

59 T. V. Kuznetsova, V. I. Grebennikov, H. Zhao, C. Derks, C. Taubitz, M. Neumann, C. Persson, M. V. Kuznetsov, I. V. Bodnar, R. W. Martin and M. V. Yakushev, A photoelectron spectroscopy study of the electronic structure evolution in CuInSe2-related compounds at changing copper content, *Appl. Phys. Lett.*, 2012, **101**, 111607.

60 S. Kashida, W. Shimosaka, M. Mori and D. Yoshimura, Valence band photoemission study of the copper chalcogenide compounds, Cu2S, Cu2Se and Cu2Te, *J. Phys. Chem. Solids*, 2003, **64**, 2357–2363.

61 J. C. W. Folmer and F. Jellinek, The valence of copper in sulphides and selenides: An X-ray photoelectron spectroscopy study, *J. Less-Common Met.*, 1980, **76**, 153–162.

62 D. Schmid, M. Ruckh, F. Grunwald and H. W. Schock, Chalcopyrite/defect chalcopyrite heterojunctions on the basis of CuInSe2, *J. Appl. Phys.*, 1993, **73**, 2902–2909.

63 D. Regesch, L. Gütay, J. K. Larsen, V. Deprédurand, D. Tanaka, Y. Aida and S. Siebentritt, Degradation and passivation of CuInSe2, *Appl. Phys. Lett.*, 2012, **101**, 112108.